Drug Delivery and Translational Research (2020) 10:594–609
https://doi.org/10.1007/s13346-020-00713-8

ORIGINAL ARTICLE

A novel strategy for glioblastoma treatment combining alpha-cyano-4-hydroxycinnamic acid with cetuximab using nanotechnology-based delivery systems

Natália N. Ferreira[1] · Sara Granja[2,3] · Fernanda Isadora Boni[1] · Leonardo M. B. Ferreira[1] · Rui M. Reis[2,3,4] · Fátima Baltazar[2,3] · Maria Palmira D. Gremião[1]

Published online: 24 January 2020

Abstract

Combination therapy that uses multiple drugs against different molecular targets should be considered as interesting alternatives for treating complex diseases such as glioblastoma (GBM). Drugs like alpha-cyano-4-hydroxycinnamic acid (CHC) and the monoclonal antibody cetuximab (CTX) are already explored for their capacity to act against different hallmarks of cancer. Previous reports suggest that the simultaneous use of these drugs, as a novel combining approach, might result in additive or synergistic effects. Therefore, advances in nanotechnology-based delivery systems will inevitably bring nano-mediated therapeutic gains to the proposed combination since they enable the association of different drugs into a single carrier. The current study provides indications that the new dual therapeutic strategy proposed, in association with nanotechnology, provides significative improvements when compared to the use of isolated drugs. Nanotechnological tools were employed by developing polymeric nanoparticles based on poly(lactic-co-glycolic acid) and chitosan for CHC encapsulation. Furthermore, these structures were conjugated with CTX by supramolecular forces. In summary, the encapsulation of the CHC drug into the nanoparticles increased its individual therapeutic capacity. In addition, conjugation with CTX seemed to enhance therapeutic efficacy, especially for U251 GBM cells. In conclusion, developed nanostructured delivery systems exhibited a set of favorable attributes and potential to be applied as a promising new alternative for GBM treatment.

Keywords Glioblastoma · α-Cyano-4-hydroxycinnamic acid · Cetuximab · Novel therapeutic strategy · Combinatory effect · Nanotechnology

Introduction

Malignant primary brain tumors comprise a heterogeneous group of diseases that arise from central nervous system (CNS) cells. Gliomas, more specifically, make up 75% of all primary brain tumors diagnosed in adults [1, 2]. Histological subtypes include astrocytomas with different malignant grades, in which glioblastoma (GBM)

✉ Maria Palmira D. Gremião
palmira.gremiao@unesp.br

Natália N. Ferreira
natalia.noronha@unesp.br

Sara Granja
saragranja@med.uminho.pt

Fernanda Isadora Boni
boni.fernanda@gmail.com

Leonardo M. B. Ferreira
miziaral@outlook.com

Rui M. Reis
ruireis.hcb@gmail.com

Fátima Baltazar
fbaltazar@med.uminho.pt

[1] School of Pharmaceutical Sciences, São Paulo State University, UNESP, Rodovia Araraquara/Jaú Km 1, Araraquara, São Paulo 14801-902, Brazil

[2] Life and Health Sciences Research Institute (ICVS), School of Medicine, University of Minho, Braga, Portugal

[3] ICVS/3B's-PT Government Associate Laboratory, Braga/Guimarães, Portugal

[4] Molecular Oncology Research Center, Barretos Cancer Hospital, São Paulo, Brazil

(grade IV) represents the most malignant and lethal form [3–5].

GBM is extremely aggressive, highly invasive, and neurologically destructive in its most hostile manifestation, with an average life expectancy ranging from 12 to 16 months and, despite the notable evolution of drug discovery, molecular biology, and technology, this statistical data has hardly changed over recent years [3, 6].

A wide range of drugs have shown potential activity against GBM, but only a few chemotherapy agents are currently approved for treatment. Although new molecular pathways are published every day, which improves our knowledge about the biology and the invasive ability of GBM cells, transposition of basic science into clinical practice has not followed this trend [5]. The biggest challenge for the scientific community today is to transpose these advances into effective treatments that take into consideration the complexities of GBM.

Sustaining proliferative signaling, metabolic reprogramming, induction of angiogenesis, activation of invasion, and the occurrence of metastasis are all well-known hallmarks of cancer, which motivate scientists to develop new drugs or new therapeutic strategies that can improve existing treatments [7–9].

Alpha-cyano-4-hydroxycinnamic acid (CHC) and the monoclonal antibody cetuximab (CTX) are already explored for their therapeutic benefits against the aforementioned concepts [10, 11].

GBM cells exhibit a high rate of aerobic glycolysis (glucose metabolism) and, consequently, lactic acid efflux is required for pH maintenance. CHC is an aromatic chemical substance of 189.2 g mol^{-1}, which has been extensively investigated for its capacity to inhibit monocarboxylate transporter (MCT) activity, especially MCT1 [12]. Their reported therapeutic benefits consist of antitumoral and antiangiogenic activity, caused by lactate buildup, which alters intracellular pH, collapses glycolytic metabolic flow, and results in glioma cell death [10, 13, 14].

Additionally, several signaling pathways are commonly disrupted in GBM [15]. Abnormal activation of the epidermal grow factor receptor (EGFR), for example, occurs in approximately 40–60% of GBM cases and its deregulated expression or activity is directly associated to tumor development, progression, metastatic spread, and high mortality rates [5, 15–20].

CTX has been pointed out as promising drug that targets EGFR-expressing tumors [21]. Its main therapeutic effects include inhibition of cell cycle progression, increased apoptosis, inhibition of invasion and metastases, and induction of antibody-dependent cell-mediated cytotoxicity, as well as inhibition of angiogenesis [22, 23].

Accumulating evidence suggests that combining two or more drugs that exhibit different action or resistance mechanisms can provide additive or synergistic effects. Previously published studies have confirmed that activation of EGFR in GBM increases both glucose uptake and lactate production, evidence that a self-regulating relationship might exist. Increased expression of different rate-limiting glycolytic genes plays a critical role in the EGFR-induced Warburg effect, which leads to an increased glucose uptake and higher lactate production in the presence of oxygen, enhancing brain tumor development [24].

Although a series of therapeutic protocols that use drug combinations have been tested, association of CTX and CHC aiming to inhibit EGFR and MCTs has not yet been studied. There is an important relationship between EGFR and tumor cell metabolism, which is particularly interesting in the context of GBM [12]. Thus, the proposed associated therapy must be thoroughly investigated.

To become a successful clinical therapy, agents must overcome not only the difficulties of reaching the anatomical location of GBM cells but also the physiologic barriers encountered on the way. Technological tools, such as nanotechnology, may be able to address such obstacles as they are proven to facilitate or even transport drugs across the blood-brain barrier (BBB) through systemic administration. Furthermore, this technology also enables the modulation of drug transportation through mucosal surfaces, which provides mucus/nanocarrier interactions and improves mucoadhesion or penetration, enabling new opportunities for more effective treatments. Another advantage of the aforementioned tools is their structural and conformational versatility, which allows the association of different drugs into a single carrier [25–27].

Applying nanoparticles to GBM treatment can be beneficial due to their biocompatibility, tumor-specific targeting, nanostructured organization, drug encapsulation and elevated protection from degradation, ability to self-assemble, enhanced permeation and retention effect, the possibility of modifying surfaces, and physicochemical manipulation that attends to specific therapeutic needs [28, 29].

Recently, nanostructured particles of poly(lactic-co-glycolic acid) (PLGA) and chitosan (CS) were proven to provide effective nose-to-brain transportation, attracting significant research attention as carrier materials for different drugs. Their unique properties contribute to the improved bioavailability of the drug in the brain [30–34].

Taking into consideration all the aforementioned challenges, and attempting to stimulate the development of new therapeutic strategies that can improve patient outcomes, the present study was undertaken to investigate the possibility of a new combined therapy using CHC and CTX against GBM cells. Furthermore, nanoparticles (NPs) based on PLGA and trimethyl chitosan were employed to efficiently encapsulate CHC into nanostructures. The physicochemical properties of CHC-loaded NPs were analyzed to measure particle size, zeta potential, surface morphology, drug loading capacity, stability, and crystallinity. CHC-loaded NPs were combined with CTX

through supramolecular forces, attempting to create a novel delivery system. Finally, the proof of concept was investigated by the analysis of therapeutic performance in vitro using cell culture carried out on SW1088 and U251 glioma cell lines.

Materials and methods

Determination of CHC and CTX IC_{50} and their combined effect against glioma cell lines

Cell lines and cell culture

Glioma cell lines U251 and SW1088, known to express MCT1 and MCT4 and overexpress the EGFR protein, were used for these studies [20, 35]. Cell line SW1088 was obtained from the American Type Culture Collection and U251 was provided by Professor Joseph Costello, California University, Neurosurgery department, San Francisco. Authentication was performed at IdentiCell Laboratories (Department of Molecular Medicine at Aarhus University Hospital Skejby, Arhus, Denmark). The cells were maintained in Dulbecco's modified Eagle's medium (DMEM 1×, high glucose; Gibco, Invitrogen), supplemented with 10% fetal bovine serum (FBS; Gibco, Invitrogen) and 1% antibiotic penicillin/streptomycin (Pen-Strep; Gibco, Invitrogen) in a humidified atmosphere at 37 °C and 5% CO_2.

Chemicals

Stock solutions of CHC (Sigma-Aldrich, St. Louis, USA), and Erbitux® (Merck KGaA, Darmstad, Germany), which contains the active substance CTX, were prepared by solubilizing them in dimethyl sulfoxide (DMSO, Sigma-Aldrich, St. Louis, USA) and DMEM, supplemented with 0.5% FBS and 1% Pen-Strep solution. The final concentration of DMSO was maintained at a maximum of 1%. All negative controls were performed using DMSO and DMEM.

Cell viability

Cell viability was assessed through the sulforhodamine B colorimetric assay (SRB) 72 h after treatment, according to the manufacturer's recommendations. Firstly, cells were plated into 96-well plates at densities of 2×10^3 for U251 and 3×10^3 for SW1088 using DMEM 10% and left to adhere overnight. Afterwards, cells were treated with increased concentrations of CHC and CTX in DMEM 0.5% FBS. Absorbance was measured using the Varioskan Flash multimode reader (Thermo Scientific, Finland), at 490 nm. The IC_{50} (value that inhibits cell growth in 50%) was calculated from at least 3 independent experiments ($n = 3$) by nonlinear regression using GraphPad Prism Software.

Combined effect of CHC and CTX against glioma cell lines

The combined effect of CTX and CHC against U251 and SW1088 was assessed by using the cell viability assay as described above. For this purpose, the treatments used in the present study consisted of the amount of CHC previously determined to induce 50% of cell death; the amount of CTX previously determined to induce 50% of cell death; and both dosages applied simultaneously as a single solution.

Development of CHC-loaded PLGA-trimethyl chitosan NPs using the nanoprecipitation technique

PLGA-chitosan NPs were prepared using a previously described nanoprecipitation method with modifications [35, 36]. First, the PLGA polymer and CHC were dissolved in 2 mL acetone. The solution was then added into 5 mL aqueous solution containing Pluronic® 188 50 mg and trimethylchitosan 5 mg, using a 5-mL syringe coupled with a 0.45 × 13 26G1/2 BD® needle and magnetic stirring. The resultant milky colloidal suspension was later evaporated to remove the acetone solvent. NPs were collected after 20 min of centrifugation at 16,000 rpm, using a Spectrafuge 16M, Labnet, Brazil, and washed with purified water to remove the unencapsulated CHC drug. For comparative purposes, empty NPs (absent of CHC drug) were obtained following the same procedure described above.

Nanoparticle characterization

Particle size, polydispersity index, zeta potential, and entrapment efficiency

Particle size and the polydispersity index (PDI) were measured using photon correlation spectroscopy (dynamic light scattering (DLS)) on a Zetasizer NanoZS (Malvern Instruments, Malvern, UK). DLS was measured on a wavelength of 532 nm at 25 °C and a detection angle of 173°. This analysis was conducted using 50 μL of NP samples diluted in 1 mL of purified water. Zeta potential (ZP) values were measured at 25 °C using Zetasizer NanoZS (Malvern Instruments, Malvern, UK) equipment with electrophoretic mobility. The amount of CHC encapsulated by the NPs was determined by using UV-VIS Spectroscopy Cary 60 (Agilent Technologies, USA), at 325 nm, using a previously obtained standard calibration curve ($y = 113.15x + 0.0016$; $r^2 = 0.999$), applying validated methodology. A known amount of CHC-loaded NPs were placed in Amicon® MWCO 100 kDa Ultra-15 Centrifugal Filter Units and centrifuged at 3000 rpm using Excelsa® II Centrifuge (Fanem®, Brazil) for 10 min. Quantification of CHC was carried out by measuring the amount of free particles deposited on the bottom of the Amicon® filter. Results are exhibited here as

the mean of tree independent determinations ($n = 3$) and their standard deviations.

Long-term NP stability

After preparation, NPs were stored in a refrigerator (8 °C) and periodically (at least once a week) analyzed for size, PDI, and zeta potential using the Zetasizer NanoZS (Malvern Instruments, Malvern, UK). Samples were appropriately diluted using ultra-purified water (1:100) and data was obtained by calculating the average of all three measurements ($n = 3$) and standard deviation.

Attenuated total reflectance Fourier transform infrared spectroscopy

Infrared spectroscopy of trimethyl chitosan, PLGA, empty NPs, and CHC-loaded NPs was performed using Fourier transform infrared (FTIR) spectrometer Vertex 70 (Bruker, Massachusetts-USA) equipped with a Golden Gate single-reflection attenuated total reflectance (ATR) accessory and a DLaTGS detector to investigate polymer-CHC interactions. Powdered samples were scanned over a wave region of 400–4000 cm^{-1}.

X-ray diffraction

X-ray diffraction (XRD) analyses of trimethyl chitosan, PLGA, empty NPs, and CHC-loaded NPs were conducted using a D5000-DIFFRAC PLUS XRD Commander (Siemens®, Germany) with monochromatic Cu-Kα radiation (λ = 15,406 Å), operating at 40 kV and 30 mA. Samples were analyzed with a detector resolution in 2θ (diffraction angle) of between 4° and 70° at room temperature with a scan step time of 0.05/min.

Field emission scanning electron microscopy

Field emission scanning electron microscopy (FEG-SEM) was performed on empty NPs and CHC-loaded NPs to analyze size and morphology. Samples were diluted (1:100 v/v), placed on a metallic holder, and left to dry at room temperature. Afterwards, samples were covered with carbon, and photomicrographs were taken at different magnifications using a JOEL-JSM-7500F coupled to the Joel Pc-100 ver.2.1.0.3. Software.

CHC-loaded NP association with CTX through supramolecular forces

PLGA-trimethyl chitosan (PLGA/TMC) NPs were combined with CTX through supramolecular association. For this purpose, 500 μL of NPs was added to 250 μL of CTX, pH was adjusted to 4.5 and 6.5, and the solution was left under magnetic stirring for 12 h. After this time period, the system was placed into an Amicon® MWCO 100 kDa filter and centrifuged for 10 min at 9000 rpm using a Heraeus Multifuge 3L-R Centrifuge (Thermo Electron Corporation, Germany). Free CTX was collected from the bottom part and quantified to calculate conjugation efficiency (%) by the indirect method, applying previous developed and validated methodology which uses reversed-phase high-performance liquid chromatography (RP-HPLC).

Biological performance

Evaluation of NP therapeutic efficacy

To evaluate therapeutic efficacy, cells were plated into 96-well plates at densities of 2×10^3 and 3×10^3 for U251 and SW1088, respectively, using DMEM 10% and left to adhere overnight. Thereafter, different treatments were applied using DMEM 0.5% FBS as negative control to compare functionalized NPs (containing 4 mM of CHC and 8.3 μg of CTX) to CHC-loaded NPs and the respective concentrations as free drug. Cell viability was assessed 72 h after treatment by the sulforhodamine B (SRB) assay. All results were normalized using their respective controls and all necessary dilutions were carried out using DMEM 0.5% of FBS.

Metabolism assay (extracellular glucose and lactate)

Quantification of extracellular glucose and lactate was carried out to evaluate the effect of the developed system on U251 and SW1088 cell metabolism. To do so, cells were plated and allowed to adhere overnight in 48-well plates at a density of 2 to 3×10^4 cells per well. After 24 h, cells were treated with DMEM without glucose for 30 min for glucose starvation. Then, different treatments were applied (DMEM as negative control, NPs, CHC-loaded NPs, associated NPs, free CHC, and free CTX). After 24 and 48 h, lactate and glucose contents were analyzed in the cell culture medium using commercial kits (Spinreact, respectively), as previously described [37–39]. Total protein, expressed as total biomass, was assessed using the SRB assay for the aforementioned time points. Results are expressed as total μg/total biomass.

Statistical analysis

Statistical analysis was performed using the GraphPad Prism Software, Version 6.0 (GraphPad Software Inc.). Differences between groups were compared using one-way analysis of variance (ANOVA), followed by the Tukey post hoc test. Results are shown as a mean ± standard deviation from a minimum of three independent experiments ($n = 3$).

Differences are considered significant at $^{**}p < 0.05$ and $^{***}p < 0.01$.

Results and discussion

Effect of α-cyano-4-hydroxycinnamic acid and cetuximab on glioma cell viability

Cell viability analysis was used to evaluate the effectiveness of alpha-cyano-4-hydroxycinnamic acid (CHC) and cetuximab (CTX) cytotoxic concentrations on U2518 and SW108 glioma cell lines: the first cell line being previously described as the most sensitive to CHC treatment and the second as the least sensitive to the same treatment [37]. Our results show that in the range of 2.5–15 mM of CHC, total biomass decreased as dosages increased for both glioma cell lines (Fig. 1a). Furthermore, when analyzing cell viability while increasing concentrations of CHC (mM), results clearly demonstrate that viability reduction was more significant between 1 and 3 mM of CHC in U151 cells and between 1 and 9 mM for SW1088 cells. Nonetheless, it is likely that increasing CHC concentration above the highest dosage applied in this study would result in further cell viability decrease.

CHC IC_{50} results obtained in the present study are in agreement with previous publications in which U251 cells presented greater sensitivity to CHC treatment [37]. When comparing these two cell lines, results showed that the IC_{50} of SW1088 for CHC was almost twice the value of U251 IC_{50}.

Regarding CTX treatment (Fig. 1b), cell viability analysis, used to investigate cytotoxic concentrations, showed the highest effective total biomass decreases at concentrations of 250 and 500 μg/mL for U251 and SW1088, respectively. IC_{50} was expressed as micrograms per milliliter, following

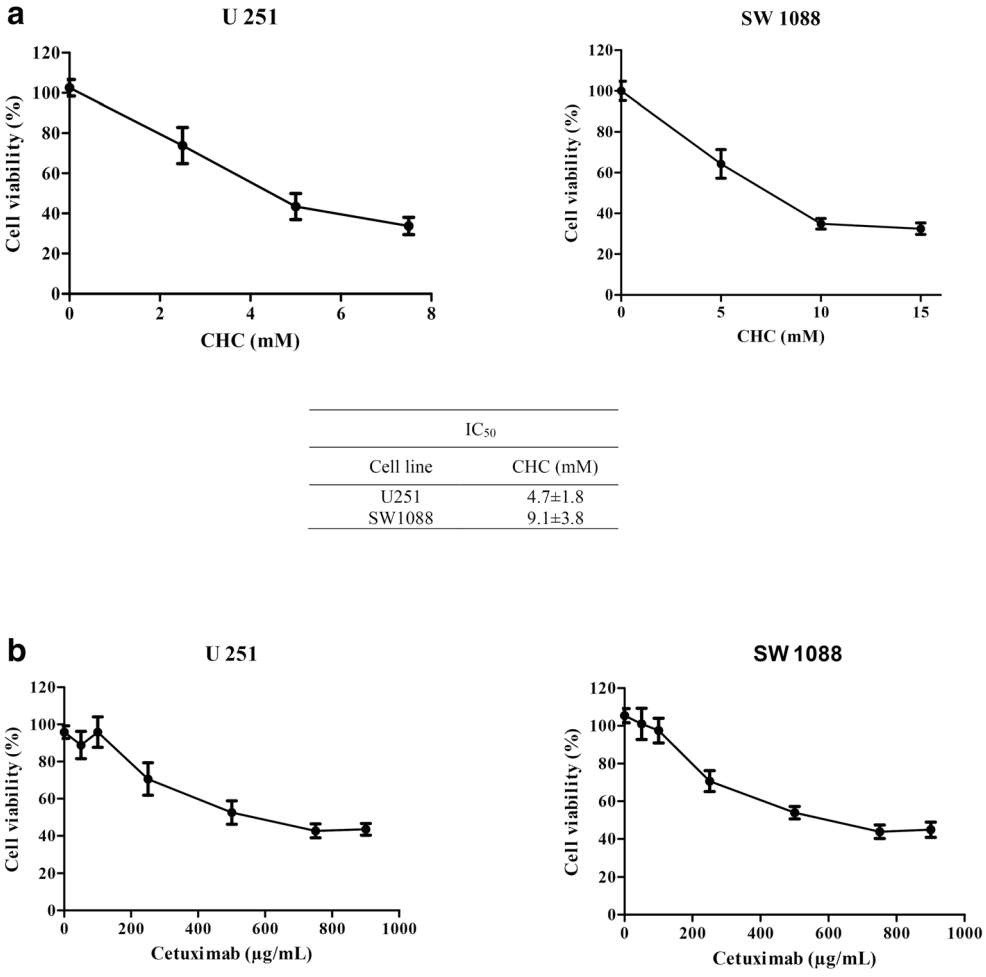

Fig. 1 **a** Cell viability values and calculated IC50 of U251 and SW1088 glioma cells in response to 72-h treatments using different concentrations of CHC. **b** and different concentrations of CTX. Values were calculated from 3 independent experiments ($n = 3$) by nonlinear regression using GraphPad Prism Software

IC_{50}	
Cell line	CHC (mM)
U251	4.7±1.8
SW1088	9.1±3.8

IC_{50}		
Cell line	CTX	
	μg/mL	mM
U251	499.5±187.4	0.00343
SW1088	636.1±30	0.00436

previous published studies, for comparative purposes [40, 41]. Differing from the results observed for the CHC regimen, treatments with increased doses of CTX did not appear to reduce cell viability in a dose-dependent manner. In fact, biomass decrease seemed to reach a plateau, where increased dosages did not result in reduction. However, biomass reduction did reach 50% and IC_{50} was calculated.

The calculated IC_{50} for CTX was approximately 500 μg/mL for U251 and 640 μg/mL for SW1088, values that correspond to 0.00343 and 0.00436 mM, respectively. Once again, the lowest IC_{50} for CTX was observed for U251 cells, while a less significant CTX effect was noticed for SW1088.

U251 and SW1088 sensitivity levels seem to follow a different pattern for each applied treatment. For instance, Martinho and co-workers, when calculating the IC_{50} for imatinib, sunitinib, and cediranib against U251 and SW1088, found that SW1088 exhibited the highest sensitivity to imatinib. Regardless of sensitivity, the main advantage of treatment with CTX, an antibody against wild type-EGFR, is that cytotoxic effects are expected for all GBM cell lines, which amplifies EGFR, even when the EGFRvIII mutation occurs [42]. Therefore, the use of such treatment seems to be very promising. After establishing the individual therapeutic potential of CHC and CTX on different glioma cell lines, we investigated their combined effect by measuring total biomass using the SRB assay.

We observed that for both cell lines, the treatment that combined the calculated IC_{50} for CHC and for CTX resulted in lower cell viability than the treatments with isolated drugs (± 50%) (Fig. 2). In addition to the fact that the combination was effective in both cell lines, the greatest promise of this treatment is based on the fact that, although cell line SW1088 was the least sensitive to both CHC and CTX drugs, herein, the combination of the two appeared to be more effective.

To the best of our knowledge, there are no published GBM treatment investigations that aim to inhibit EGFR by using CTX in association with a MCT inhibitor, such as CHC. Thus, the obtained results may represent a promising alternative to be further explored.

Nevertheless, it is very important to address that GBM treatment displays peculiar challenges which need to be carefully evaluated and studied to ensure positive results. We cannot forget that, apart from the heterogeneity of GBM, the blood-brain barrier and mucosal surfaces are also major hurdles for drug permeability that should not be neglected. This fact might explain why a series of new treatments are suggested daily, but few of them show promising results in clinical trials.

To overcome these obstacles, advances in material engineering and pharmaceutical technology may offer valuable tools to explore new routes for drug administration as intranasal route. When a chemical substance is included into a new carrier material, such as polymeric nanoparticles, it acquires new properties, oftentimes, distinct from the isolated drug. That said, the approach studied here can improve drug stability, solubility, absorption, and even therapeutic efficacy, due to the novel characteristics provided by the carrier platform. Given the complexity of GBM, new therapeutic protocols must be associated or improved through new insights in pharmaceutical technology to provide strongly relevant and favorable therapies.

Evidences that nanotechnology can enhance the direct transport to CNS are noticeable and crucial, since it not only allows drug protection, but, most importantly, it improves the uptake by the olfactory mucosa [43–47].

CHC-loaded PLGA-trimethyl chitosan NPs

The main challenge in the development of new polymeric systems for drug delivery applications is the control of all

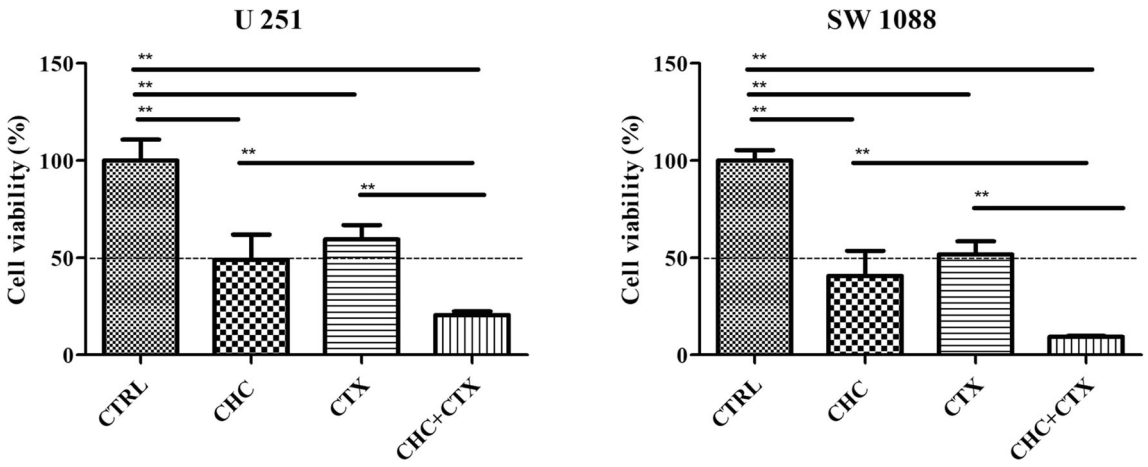

Fig. 2 Combined effect of using both CHC and CTX against glioma cell lines U251 and SW1088. Results are expressed as mean –SD; $n = 6$. CHC group received the amount of drug that induce 50% of cell death; CTX group received the amount of drug to induce 50% of cell death and CHC+CTX received both dosages applied simultaneously as a single solution. One-way analysis of variance followed by Tukey's multiple comparison test was used for statistical analysis ($p < 0.05$). Differences $p < 0.05$ were considered statistically significant (**)

critical attributes involved in obtaining these systems. Modification of some parameters cause crucial changes in characteristics such as size, drug entrapment, zeta potential, and so on [48]. Thus, preliminary tests were employed to evaluate the PLGA ratio of lactide versus glycolide, CHC concentration, temperature, and stirring speed used for the production of NPs. After this screening, NPs were produced using PLGA 85:15, 60 °C, stirring speed of 1000 rpm, and CHC concentration of 2 mg mL^{-1}, an experimental condition that generates stable particles with low PDI, zeta potential values between + 30 and + 50 mV, and high CHC entrapment.

NP characterization

Particle size, polydispersity index, zeta potential, and entrapment efficiency

Particle size and polydispersity index (PDI) are critical attribute for NP development as it can determine important properties such as surface area and packing density [49]. In addition, they may affect the in vivo performance and distribution of NPs [50]. Developed systems of unloaded CHC (referred to as empty NPs throughout the manuscript) exhibited a size close to 250 ± 28 nm, while CHC-loaded NPs exhibited an increased size of 350 ± 40 nm. For PDI results, values were noticeably higher for CHC-loaded NPs (0.35 ± 0.03) than for empty NPs (0.2 ± 0.05). Low PDI is desired in this case since it characterizes homogeneous particle size distribution [51]. In fact, the nanoprecipitation technique applied to develop polymeric nanoparticles often enables the formation of small structures with narrow unimodal distribution [52].

Zeta potential (ZP) is a critical parameter that is related to the occurrence of supramolecular interactions in particle dispersion and stability of colloidal systems [53]. Since ZP values close to zero indicate high tendency for agglomeration [54], our interest was to obtain values around or even higher than + 30 mV, which is important for system stability and distributes chitosan polymers on the outermost particle surface, leading to the formation of cationic particles [55]. The empty NPs exhibited a ZP value of 50 ± 8 mV, while CHC-loaded NPs presented a ZP value of 45 ± 3 mV. Measuring entrapment efficiency (EE%) is fundamental to determine system applicability and therapeutic efficacy; the applied methodology provided around 87 ± 8.5% of drug entrapment. The high drug entrapment rate obtained here was expected, since the hydrophobic drugs were encapsulated using the nanoprecipitation method [56, 57].

Long-term NP stability

The stability of NPs can be reflected by their morphology, average size, and size distribution. Thus, periodically over a 3-month period, portions of empty NPs and CHC-loaded NPs were taken, diluted using Milli-Q water, and measured for characteristics of physical stability using DLS (size, PDI, and ZP) (Fig. 3). According to the results, while empty NPs exhibited a size close to 250 nm throughout the 3-month analysis, the CHC-loaded NPs exhibited a size of 350 nm. In regard to size variability among the different weeks of analysis, size stability of empty NPs was acquired after 2 weeks and was maintained until the end of the 3-month analysis period. On the other hand, when CHC was loaded, the stabilization period was longer, only being acquired around week 6 of the analysis period. Furthermore, NP size appears to have had the same profile over the 3-month period, regardless of CHC loading. For PDI results, significantly higher values were found in the presence of the CHC drug, which was expected once increased size was noticed along the analyzed period.

The variability of ZP was observed from the very beginning of the analysis period (between + 30 and + 55 mV), emphasizing system stability and presence of chitosan TMC on the outermost particle surface. Unlike previous results, empty NPs exhibited reduction in ZP between weeks 4 and 8. However, this reduction did not reach critical levels that could possibly affect stability. On the other hand, CHC-loaded NPs did not show any significant changes.

Its well-known that nanoparticulate systems may have their properties modified over the time. CHC-loaded NPs appeared to show more stable values during the evaluated period than empty NPs, leading us to believe that the interaction between the CHC drug and the developed particle could provide additional stability, modifying the kinetic aspects of stabilization [58].

Attenuated total reflectance Fourier transform infrared spectroscopy

Fourier transform infrared (FTIR) analysis was conducted as a preliminary evaluation of the molecular structure of NP constituents and of the possible chemical interactions between NPs and the CHC drug. The CHC drug spectrum showed broad and strong signals of the –OH hydroxyl group, at around 3300 cm^{-1}, and it also exhibited stretching of –COOH carboxylic acid as a strong broad signal ranging between 2500 and 3300 cm^{-1} (Fig. 4). These signs were also overlapped by an intermediate –CH stretching of alkene (C showing sp2 hybridization). Nitrile –CN exhibited a typically weak sign, stretching at 2200 cm^{-1}. Signals assigned to C–C and C–H bands were observed between 1567 and 1295 cm^{-1}, corroborating with previously published CHC data [59]. From the PLGA spectrum, a C–O–C stretching peak was observed at around 1088 cm^{-1}. C–H stretching in methyl groups was noticed at around 1460 cm^{-1}, while C=O stretching vibration was noticed at 1750 cm^{-1}. C–H, $–CH_2$, and $–CH_3$ resulted in subtle signals between 2800 and 3000 cm^{-1} [60].

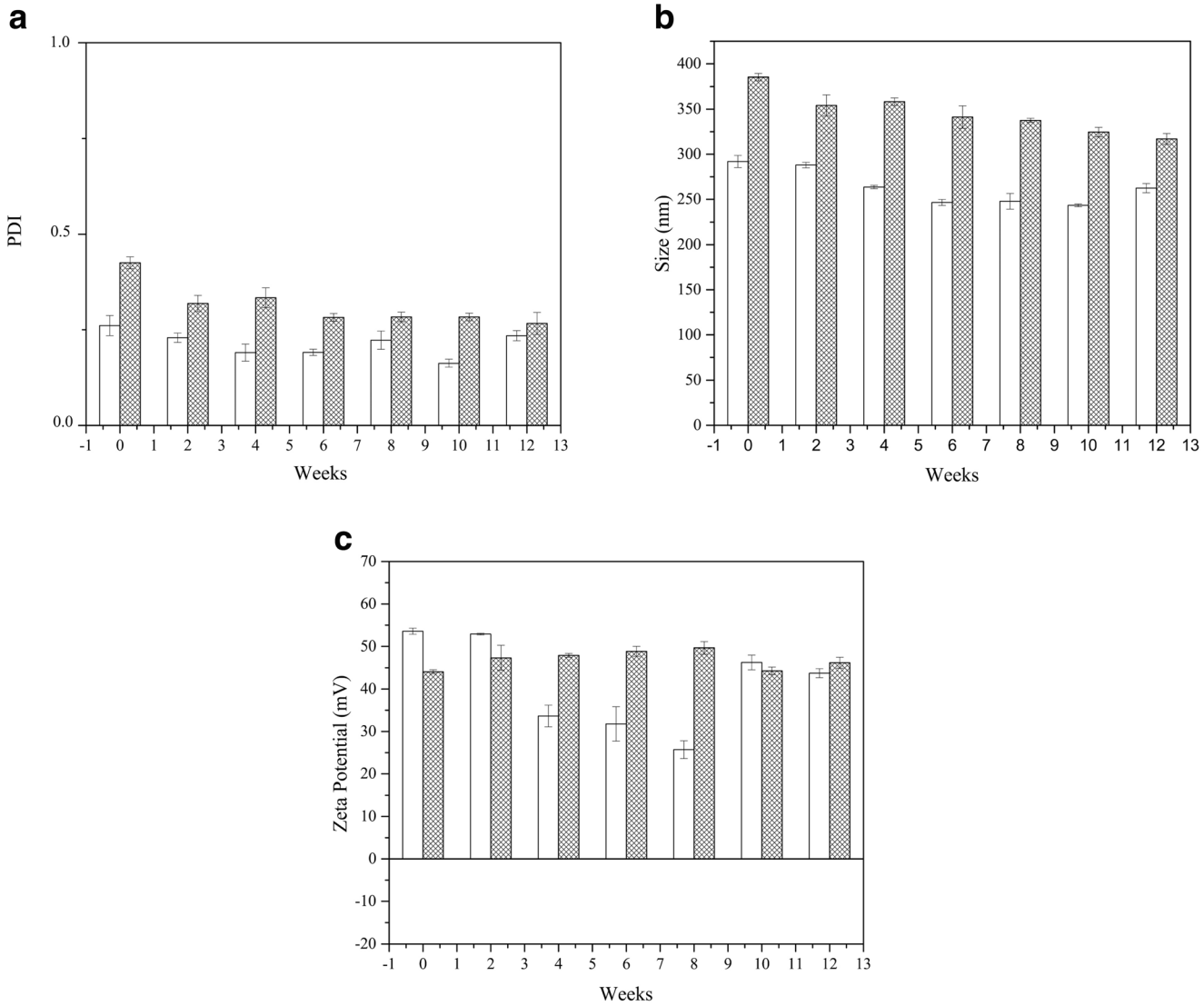

Fig. 3 Long-term stability of empty NPs (white bars) and CHC-loaded NPs (filled bars). Periodically, an aliquot of prepared NPs was pulled, diluted using MiliQ water, and assessed for the stability if their physical properties using DLS. **a** Size (nm), **b** PDI, and **c** Zeta Potential (mV). White columns represent empty NPs and dotted columns represent CHC-loaded NPs

Methylation of chitosan amino groups to acquire TMC was accomplished by using methyl at an elevated temperature and a strong alkaline environment to bind the acid generated during the reaction [61]. Main bands are considered to characterize TMC. One of them, around 3400 cm^{-1}, is assigned to the OH group stretching vibration [62]. This region also encompasses amine N–H stretching; thus, tertiary amines are easily differentiated from primary and secondary amines. Since TMC is synthesized by substituting its amino group, when a high degree of substitution is achieved, this signal becomes very subtle or may even disappear, as we can observe from the results presented in this study.

The FTIR spectra of empty NPs (Fig. 4(d)) showed peaks similar to those of PLGA and TMC. For instance, C=O stretching vibration at 1750 cm^{-1}, which occurred in the PLGA spectrum, also appeared for empty NPs. Regardless of the presence or not of CHC, new significant peaks appeared at 2880 cm^{-1} and 1090 cm^{-1}, which indicates that they are associated to the PLGA-TMC interaction.

CHC-loaded NPs presented a spectrum similar to the empty NPs. The typical signal for CHC, around 2200 cm^{-1}, is associated with the vibrational CN and does not appear in CHC-loaded NP spectrum. Therefore, the drug may have been associated into the polymer chains interacting with the polymer matrix by supramolecular forces.

X-ray diffraction

In order to comparatively study the crystallinity of CHC, PLGA, TMC, OCS, and developed NPs, X-ray diffraction

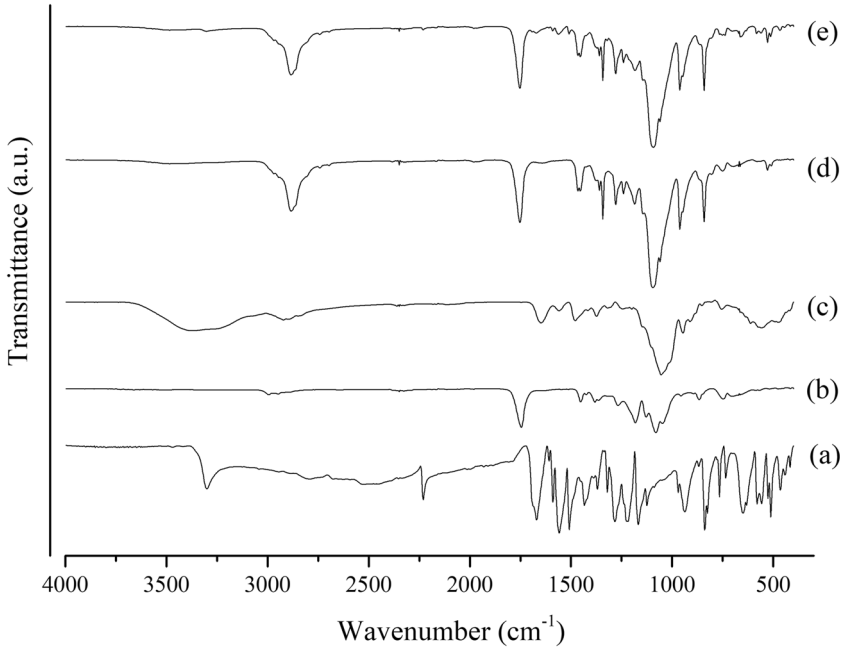

Fig. 4 ATR-FTIR spectra of **a** CHC, **b** PLGA, **c** TMC, **d** empty NPs, and **e** CHC-loaded NPs^{-1}

(XRD) analyses were carried out and the patterns observed are presented below. According to Fig. 5, with the exception of the CHC drug, patterns of all isolated materials showed few peaks and wide halos, indicating typical behavior of amorphous materials. Generally, PLGA is recognized as an amorphous material [63]. On the other hand, CHC exhibits several intense and well-defined peaks due its crystalline characteristics. Peaks are displayed mainly in low values of 2θ, at about 19.4°, 24.6°, and 27.95°. However, one peak was noticed at 57.9°. In regard to TMC, a semi-crystalline structure with a very low crystallinity level is expected usually where crystalline regions do not exhibit sufficiently detectable X-ray scattering intensities.

The pattern of empty NPs shows two peaks in low values of 2θ, at 19.1 and 23.1°, highlighting the occurrence of structural changes for NP formation, which probably occurred due to the rearrangement of the polymer chains, resulting in the development of structures with higher levels of organization. For CHC-loaded NPs, the XRD pattern clearly shows an intense and well-defined peak at $2\theta = 27.9°$, which indicates the presence of CHC in the polymeric structure.

Field emission scanning electron microscopy

Representative images of empty NPs and CHC-loaded NPs at different magnifications, shown in Fig. 6, highlight the formation of spherical and uniformly shaped particles, including a mixed population of sizes. Acquisition of empty NPs through the recorded image was in the range of 150 nm. PLGA usually provides, because of its amphiphilic character, formation of core-shell spherical structures due to its micelle-like behavior. Especially for nanoprecipitation technology, nanoparticle assembly is a direct function of block size and phase separation, which can be reasonably predicted a priori. Thus, size and morphology of the developed nanoparticles can be controlled by tuning the block lengths [64].

Encapsulation of the CHC drug into the NPs (CHC-loaded NPs) resulted in formation of larger particles which, contrarily to the empty NPs, do not exhibit perfect spherical, well-defined shapes. These results are in agreement with size and PDI determinations that had been previously recorded using DSL measurements. Interestingly, regardless of CHC presence, size, measured by SEM, was lower than hydrodynamic particle size recorded from DLS. This fact can be explained by the presence of hydrated layers found in NPs evaluated by light scattering, but absent in dry conditions imposed by SEM. Differences in particle size measured by DLS and SEM were previously reported and attributed to distinctions in measurement conditions for sample preparation [63, 65].

Association between CHC-loaded NPs and CTX by supramolecular forces

Over the last few years, substantial efforts have been made to develop delivery systems that contain target molecules attached to their surface. Several studies have focused on antibody conjugates to develop highly specific systems [66]. Since such molecules are naturally polyelectrolytes, supramolecular associations can be considered for the conjugation procedure. Supramolecular interactions are non-covalent forces that, although less energetic than covalent bonds, enable a wide set of advantages to design drug delivery systems and

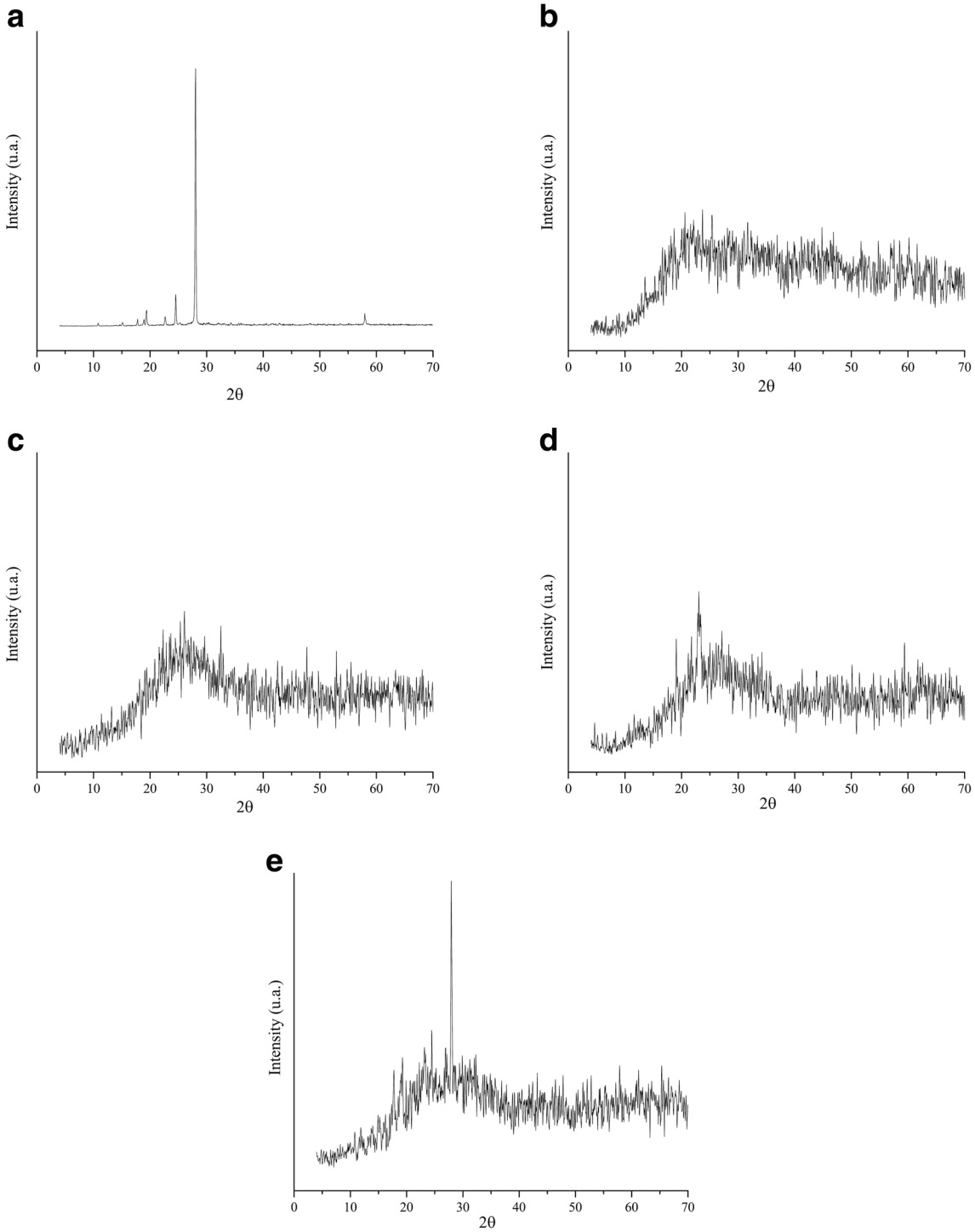

Fig. 5 X-ray diffraction patterns of isolated materials. **a** CHC; **b** PLGA; **c** TMC, and developed **d** empty NPs, **e** CHC-loaded NPs

can be responsible for the organization of nanostructured systems at the nanobiointerface [67]. These interactions are weak by nature and are significantly affected by pH. Therefore, we explore the association between CHC-loaded NPs and CTX at pH 4.0 and 6.0.

Interactions at pH 4.0 resulted in about 53% of CTX associated with the system. On the other hand, the increase in pH improved these interactions reaching an efficiency of 85% at pH 6.0. The acquired results may be advantageous for the intended application, since tumor microregions and nasal environment tend to show slightly acidic pH values (around 6.0) when compared to most physiological pH [68]. Therefore, we selected this condition of preparation for future studies.

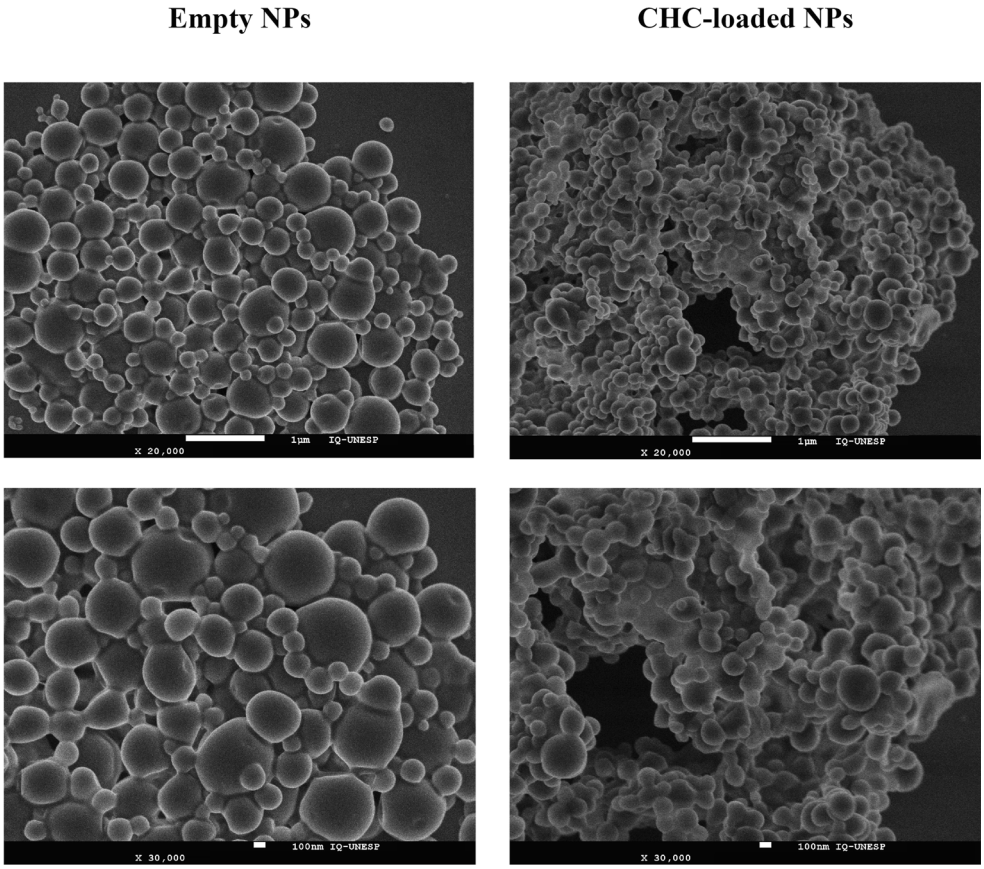

Fig. 6 SEM micrographs exhibit surface morphology of both empty and CHC-loaded NPs at different magnifications

Biological performance

Understanding NP interactions with cells and how those interactions can modulate biological performance is essential to explore NP applications. This assessment can help NP design efficiently and can be used as a starting point to investigate new alternatives for drug administration.

NPs are able to interact with cells and extracellular environments promoting a series of biological effects that depend on physicochemical characteristics, which further determine the efficacy of intended outcomes. Evaluating biocompatibility becomes essential to assure safe use of the intended treatments [69]. As stated by all regulatory agencies, it is important that drug delivery systems, no matter how attractive they seem to be, because of the therapeutic effect they provide, hold no weight unless considered adequately biocompatible. Importantly, drug delivery systems are considered biocompatible when cell viability is equal or greater than 80% [69].

Firstly, we determined cell biocompatibility and cell viability of developed nanoparticles by using increased concentrations (0.5 to 1.5 μL of NPs) after 72 h. We chose to work with nanoparticle amounts, since this will facilitate the future use of different drugs and concentrations. Herein, empty NPs as well as CHC-loaded nanoparticles were used in an attempt to find a specific dosage where empty NPs would not reduce cell viability and CHC-loaded nanoparticle would result in significant reduction of total biomass (Fig. 7a). As we can observe, for volumes of up to 5 μL of empty NPs, there was no significant reduction of cell viability for both U251 and SW1088 cell lines. Notably, increasing concentrations (0.5, 1, and 5 μL) of NPs did not promote cell viability reduction for the U251 cell line, suggesting that the reduction observed for CHC-loaded NPs may be attributed to CHC encapsulation rather than the NPs' components.

For SW1088, the results described above were also noticed. Among all applied concentrations of NPs, none was able to promote a significant cell viability decrease, reinforcing system biocompatibility. On the other hand, 5 to 15 μL of CHC-loaded PLGA/TMC NPs resulted in considerable cell viability decrease (50% or more). Importantly, these results reinforce, once again, that SW1088 is less sensitive than U251.

Following the investigation of biological performance, conjugated NPs (5 μL) were further examined to determine if the therapeutic effect they provide is more or less efficient than CHC-loaded NPs and free drugs, at the same concentration. According to the acquired data (Fig. 7b), the encapsulation of the CHC compound into developed NPs alone resulted in significant increase of therapeutic activity for both U251 and SW1088 cell lines, higher than that of the free CHC drug at the same concentration. However, the reduction of cell viability was more pronounced for U251 cells. The superiority

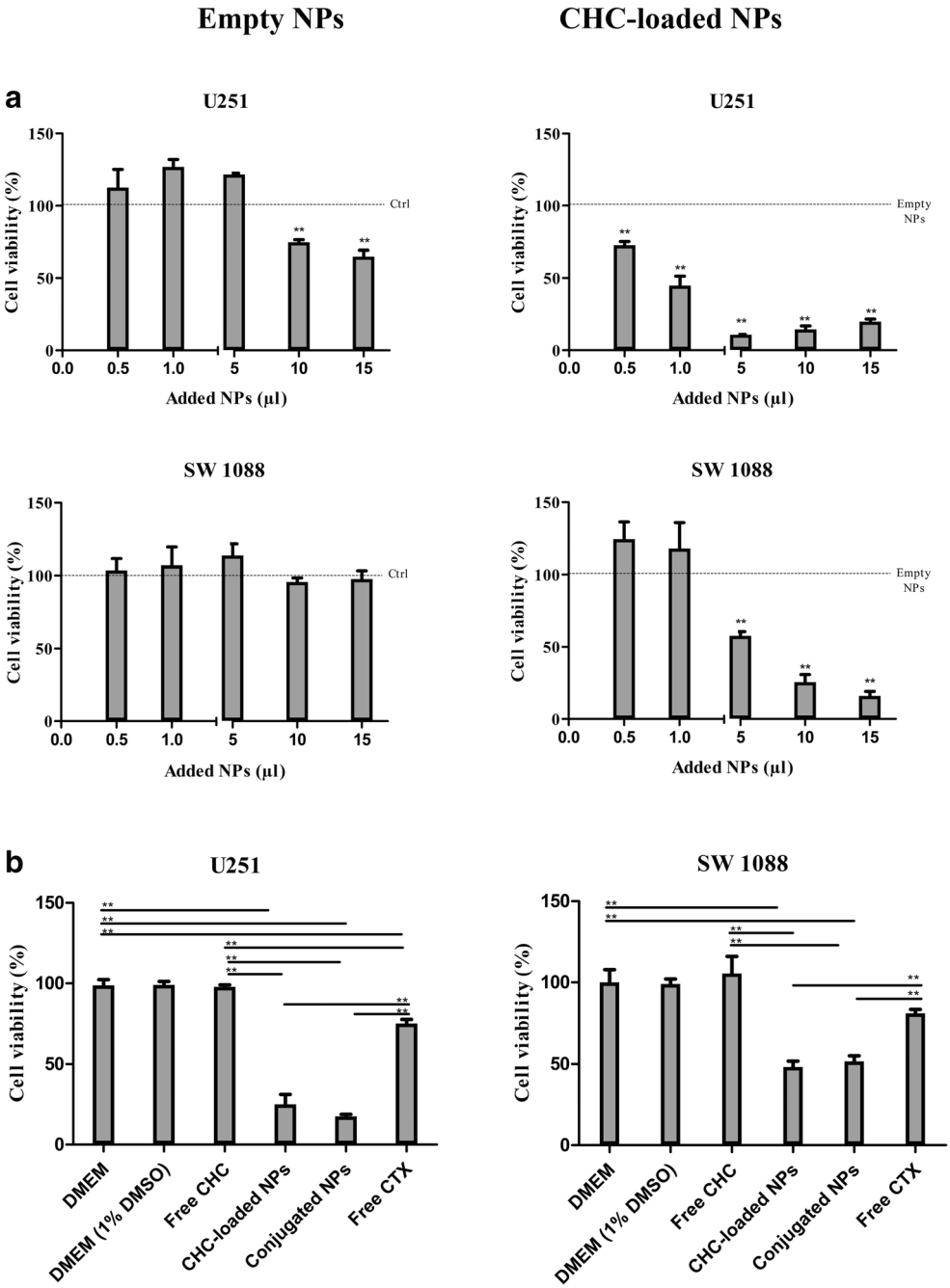

Fig. 7 **a** Cell biocompatibility and cell viability results of empty NPs and CHC-loaded NPs against glioma cell lines U251 and SW1088. **b** Conjugated NPs therapeutic efficacy against glioma cell lines U251 and SW1088 compared to isolated treatments. Results are expressed as mean –SD; $n = 6$. Differences $p < 0.05$ between the control and applied treatment were considered statistically significant (**)

observed for CHC-loaded NPs can be correlated with the CHC solubility or mechanism of action. According to its hydrophobic nature, obtaining a homogeneous CHC solution can be difficult. Therefore, the developed NP structures, as well as other previously proposed delivery systems, may allow the slow release of CHC, increasing drug bioavailability and, so far, increasing potency [70]. Another hypothesis consists on the fact that NPs could promote CHC entry into the cell. In this way, CHC probably will compromise the entry of pyruvate into the mitochondria and normal cell respiration at much lower concentrations [71]. A combination of the aforementioned effects is also a possibility that should not be excluded.

Comparing both free drugs (CHC and CTX), no significant statistical difference was found for cell viability reduction or for the respective controls. Contrarily, conjugated NPs resulted in a considerable decrease of cell viability in both studied cell lines. Interestingly, conjugation with CTX seemed to improve therapeutic efficacy for U251, while neither CHC-loaded NPs nor conjugated NPs presented any statistical evidences of treatment improvements for SW1088 cells. Once again, the higher sensitivity of U251 to the applied treatments was clearly observed.

Concerning the reduction in cellular viability produced by the simultaneous application of free CHC and CTX in the initial studies, two hypotheses can be further investigated.

On the one hand, encapsulation of CHC may have enhanced its therapeutic activity and, as a result, conjugation with CTX did not provide significant benefits. On the other hand, taking into account that CTX acts in the transmembrane of cell domains, its association with nanoparticles by supramolecular forces did not provide the full site of action availability. In this particular case, an alternative CTX conjugation procedure that uses new protocols to ensure a novel antibody assembly into the nanostructure (e.g., covalent bonds) may effectively increase therapeutic benefits.

Next, extracellular glucose and lactate levels were analyzed to explore the spectrum of encapsulated CHC activity over cell metabolism. Regarding U251 cells, at 24 h, CHC and conjugated NPs exhibited higher glucose consumption than their respective negative controls. This behavior can be associated with initial efforts to compensate metabolic pathways (Fig. 8a). On the other hand, at 24 h, extracellular lactate was higher for all applied treatments than their respective controls, with the exception of free CHC. The acquired results were expected since CHC, when used as a free drug, acts as a competitive lactate inhibitor outside the cell. However, when encapsulated and also internalized into GBM cells, it may inhibit mitochondrial functions and stimulate glycolysis [71].

Glucose consumption was higher at 48 h than at 24 h for CHC-loaded NP and CHC treatments, although this increase is also evident for empty NPs and for conjugated NPs. No significant difference was found between 24 and 48 h for extracellular lactate. Since U251 cells are known to be highly glycolytic, the glucose consumption noticed for CHC-loaded NPs and CHC between 24 and 48 h should be accompanied by higher production of extracellular lactate. As this fact was not observed, lactate efflux to the extracellular environment could have been hampered by CHC activity, which may be related to the drug initially released from NPs.

For the SW1088 cell line (Fig. 8b), at 24 h, glucose consumption was notoriously low for CTX treatment, but higher

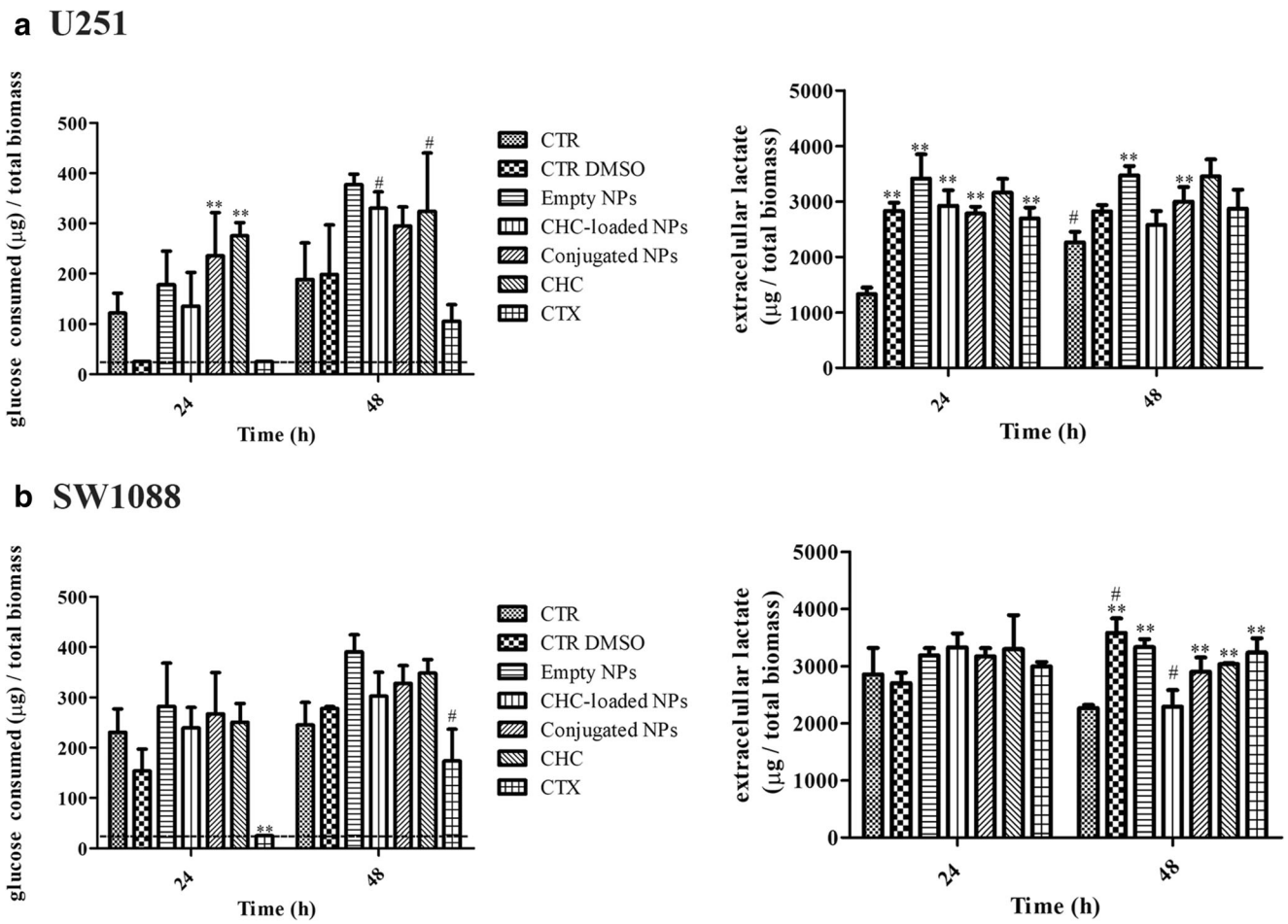

Fig. 8 Glucose consumption and extracellular lactate (μg) /total biomass of (**a**) U251 and (**b**) SW1088 cells applying different treatments. CTR: negative control received DMEM 10% FBS; CTR DMSO: DMEM 10% FBS + 1% DMSO; NPs: empty NPs diluted in DMEM 10% FBS; CHC-loaded NPs: CHC-loaded NPs diluted in DMEM 10% FBS; Conjugated NPs: CTX conjugated CHC-loaded NPs; CHC: free CHC diluted in DMEM 10% FBS + 1%DMSO; CTX: free CTX diluted in DMEM 10% FBS. Results are representative of the three independent experiments, each one in triplicate; $^{**}p < 0.05$ Treatment versus control. # $p < 0.05$ 24 and 48 h. Dotted line represents that glucose concentration was lower than quantification limit

at 48 h. Concerning extracellular lactate quantification at 24 and 48 h, while an increase could be noticed for the CTR DMSO, CHC-loaded NPs exhibited reduction of extracellular lactate levels, likely due to the aforementioned CHC activity.

Analyzing these results together, the increased glucose consumption between 24 and 48 h appeared to be more evident for U251 than for SW1088. On the other hand, extracellular lactate for both cell lines remained markedly unchanged between 24 and 48 h, with the exception of CHC-loaded NPs applied to SW1088 cells.

Conclusions

The present study has provided the first in vitro investigation of a dual therapeutic strategy combining CHC and CTX against glioma cell lines SW1088 and U251. According to the acquired results, the applied combinatory regimen provided significantly greater cell viability reduction than the isolated drugs.

Nanotechnology has brought many important advances to the field of cancer treatment, providing greater therapeutic efficiency when compared to the use of isolated drugs. Considering that nanostructured systems are able to optimize therapeutic effect, especially for complex pathological processes such as GBM, we successfully designed an innovative polymeric delivery system based on PLGA/trimethyl chitosan for CHC encapsulation by the nanoprecipitation technique. The developed CHC-loaded NPs contained chitosan on its outermost surface, resulting in a positive ZP, and a high percentage of CHC was loaded into the NPs. SEM images revealed a spherical morphology with uniform shape of several nanosizes. Furthermore, CHC-loaded NPs were optimally conjugated with CTX through supramolecular forces at pH 6.0. In vitro protocols showed that encapsulation of CHC into polymeric NPs results in a significant increase in therapeutic activity for both of the cell lines studied. Regarding the conjugated NPs, therapeutic gains were more evident for U251 cells. However, an apparent decrease in cell viability also seems to occur for SW1088 cells. Additional aspects can be modulated in an attempt to deeper investigate this effect further.

Analysis of cell metabolism by extracellular glucose and lactate quantification established that encapsulated CHC may have acted by different mechanisms. As a free drug initially released from NPs, they could impair lactate efflux. However, when internalized, CHC exhibited intracellular activity, compromising normal mitochondrial activity at much lower concentrations. Therefore, the applied innovation may potentiate its therapeutic capacity.

Taking into consideration all of the aforementioned results, we anticipate that the developed CHC-loaded NPs and conjugated NPs exhibit a set of favorable attributes that make them promising alternatives to be further explored and considered in GBM treatment. Importantly, future studies should evaluate release profiles, as well as in vivo performance of the clinical application of the proposed treatments.

Acknowledgments The authors would like to thank the National Institute of Science and Technology in Pharmaceutical Nanotechnology: a transdisciplinary approach INCT-NANOFARMA, which is supported by the "Fundação de Amparo e Pesquisa do Estado de São Paulo" (FAPESP, Brazil), grant no. 2014/50928-2, and by "Conselho Nacional de Desenvolvimento Científico e Tecnológico" (CNPq, Brazil), grant no. 465687/2014-8.

Authors' contributions Conceptualization, methodology, and data acquisition: N.N.F.; S.G.; F.I.B.; L.M.B.F.; resources: M.P.D.G.; F.B.; R.M.R.; data curation: all authors; writing of original draft: N.N.F; writing-review and editing: all authors; supervision: M.P.D.G.; F.B.; R.M.R.; project administration and funding acquisition: N.N.F; M.P.D.G.; F.B.; R.M.R.; data analysis and scientific discussion: all authors

Funding information This work was financially supported by Fundação de Amparo e Pesquisa do Estado de São Paulo (FAPESP), grant nos. 2017/16324-0, 2016/09671-3, and 2018/04546-1. SG received a fellowship from FCT, ref. SFRH/BPD/117858/2016. This work was also developed under the scope of the project NORTE-01-0145-FEDER-000013, supported by the Northern Portugal Regional Operational Programme (NORTE 2020) under the Portugal Partnership Agreement, through the European Regional Development Fund (FEDER), and through the Competitiveness Factors Operational Programme (COMPETE) and by National funds, through the Foundation for Science and Technology (FCT), under the scope of the project POCI-01-0145-FEDER-007038.

Compliance with ethical standards

Conflict of interest The authors declare that they have no conflict of interest.

References

1. Ostrom QT, Gittleman H, Liao P, Vecchione-Koval T, Wolinsky Y, Kruchko C, et al. CBTRUS statistical report: primary brain and other central nervous system tumors diagnosed in the United States in 2010–2014. Neuro-Oncology. 2017;19:v1–v88. https://doi.org/10.1093/neuonc/nox158.
2. Lapointe S, Perry A, Butowski NA. Primary brain tumours in adults. Lancet. 2018;392:432–46. https://doi.org/10.1016/S0140-6736(18)30990-5.
3. Maher EA, Furnari FB, Bachoo RM, Rowitch DH, Louis DN, Cavenee WK, et al. Malignant glioma: genetics and biology of a grave matter. Genes Dev. 2001;15:1311–33. https://doi.org/10.1101/gad.891601.
4. Hekmatara T, Bernreuther C, Khalansky A, Theisen A, Weissenberger J, Matschke J, et al. Efficient systemic therapy of rat glioblastoma by nanoparticle-bound doxorubicin is due to antiangiogenic effects. Clin Neuropathol. 2009;28:153–64. https://doi.org/10.5414/NPP28153.
5. Veliz I, Loo Y, Castillo O, Karachaliou N, Nigro O, Rosell R. Advances and challenges in the molecular biology and treatment of glioblastoma—is there any hope for the future? Ann Transl Med. 2015;3:7. https://doi.org/10.3978/j.issn.2305-5839.2014.10.06.
6. Karsy M, Yoon N, Boettcher L, Jensen R, Shah L, MacDonald J, et al. Surgical treatment of glioblastoma in the elderly: the impact of complications. Neuro-Oncol. 2018;138:123–32. https://doi.org/10.1007/s11060-018-2777-9.

7. Hanahan D, Weinberg RA. Hallmarks of cancer: the next generation. Cell. 2011;144(5):646–74. https://doi.org/10.1016/j.cell.2011.02.013.
8. Agnihotri S, Zadeh G. Metabolic reprogramming in glioblastoma: the influence of cancer metabolism on epigenetics and unanswered questions. Neuro-oncol. 2015;18:160–72. https://doi.org/10.1093/neuonc/nov125.
9. Keller S, Schmidt MHH. EGFR and EGFRvIII promote angiogenesis and cell invasion in glioblastoma: combination therapies for an effective treatment. Int J Mol Sci. 2017;18:1295–314. https://doi.org/10.3390/ijms18061295.
10. Miranda-Goncalves V, Granja S, Martinho O, Honavar M, Pojo M, Costa BM, et al. Hypoxia-mediated upregulation of MCT1 expression supports the glycolytic phenotype of glioblastomas. Oncotarget. 2016;7:46335–53. https://doi.org/10.18632/oncotarget.21761.
11. Taylor TE, Furnari FB, Cavenee WK. Targeting EGFR for treatment of glioblastoma: molecular basis to overcome resistance. Curr Cancer Drug Targets. 2012;12:197–209. https://doi.org/10.2174/156800912799277557.
12. Bannister TD. Inhibitors of lactate transport: a promising approach in cancer drug discovery. In: Reference module in biomedical sciences; Encyclopedia of cancer. 3ed ed; 2019. p. 266–78. https://doi.org/10.1016/B978-0-12-801238-3.64996-6.
13. Miranda-Gonçalves V, Reis RM, Baltazar F. Lactate transporters and pH regulation: potential therapeutic targets in glioblastomas. Curr Cancer Drug Targets. 2016;16:388–99. https://doi.org/10.2174/1568009616666151222150543.
14. Caruso JP, Koch BJ, Benson PD, Varughese E, Monterey MD, Lee AE, et al. pH, lactate, and hypoxia: reciprocity in regulating high-affinity monocarboxylate transporter expression in glioblastoma. Neoplasia. 2017;19:121–34. https://doi.org/10.1016/j.neo.2016.12.011.
15. Zahonero C, Sanchez-Gomez P. EGFR-dependent mechanisms in glioblastoma: towards a better therapeutic strategy. Cell Mol Life Sci. 2014;7:3465–88. https://doi.org/10.1007/s00018-014-1608-1.
16. Hicks MJ, Chiuchiolo MJ, Ballon D, Dyke JP, Aronowitz E, Funato K, et al. Anti-epidermal growth factor receptor gene therapy for glioblastoma. PLoS One. 2016;11:e0162978. https://doi.org/10.1371/journal.pone.0162978.
17. Zorzan M, Giordan E, Redaelli M, Caretta A, Mucignat-Caretta C. Molecular targets in glioblastoma. Future Oncol. 2015;11(9):1407–20. https://doi.org/10.2217/fon.15.22.
18. Binder ZA, Thorne AH, Bakas S, Wileyto EP, Bilello M, Akbari H, et al. Epidermal growth factor receptor extracellular domain mutations in glioblastoma present opportunities for clinical imaging and therapeutic development. Cancer Cell. 2018;34:163–77. e7. https://doi.org/10.1016/j.ccell.2018.06.006.
19. Bax DA, Gaspar N, Little SE, Marshall L, Perryman L, Regairaz M, et al. EGFRvIII deletion mutations in pediatric high-grade glioma and response to targeted therapy in pediatric glioma cell lines. Clin Cancer Res. 2009;15:5753–61. https://doi.org/10.1158/1078-0432.CCR-08-3210.
20. Viana-Pereira M, Lopes JM, Little S, Milanezi F, Basto D, Pardal F, et al. Analysis of EGFR overexpression, EGFR gene amplification and the EGFRvIII mutation in Portuguese high-grade gliomas. Anticancer Res. 2008;28:913–20.
21. Fukai J, Nishio K, Itakura T, Koizumi F. Antitumor activity of cetuximab against malignant glioma cells overexpressing EGFR deletion mutant variant III. Cancer Sci. 2008;99:2062–9. https://doi.org/10.1111/j.1349-7006.2008.00945.x.
22. Vincenzi B, Schiavon G, Silletta M, Santini D, Tonini G. The biological properties of cetuximab. Crit Rev Oncol Hematol. 2008;68:93–106. https://doi.org/10.1016/j.critrevonc.2008.07.006.
23. Golay J, Introna M. Mechanism of action of therapeutic monoclonal antibodies: promises and pitfalls of in vitro and in vivo assays. Arch Biochem Biophys. 2012;526:146–53. https://doi.org/10.1016/j.abb.2012.02.011.
24. Yang W, Zheng Y, Xia Y, Ji H, Chen X, Guo F, et al. ERK1/2-dependent phosphorylation and nuclear translocation of PKM2 promotes the Warburg effect. Nat Cell Biol. 2012;14:1295–304. https://doi.org/10.1038/ncb2629.
25. Ferreira LMB, Alonso JD, Kiill CP, Ferreira NN, Buzzá HH, Martins de Godoi DR, et al. Exploiting supramolecular interactions to produce bevacizumab-loaded nanoparticles for potential mucosal delivery. Eur Polym J. 2018;103:238–50. https://doi.org/10.1016/j.eurpolymj.2018.04.013.
26. Tzeng SY, Green JJ. Therapeutic nanomedicine for brain cancer. Ther Deliv. 2013;4:687–704. https://doi.org/10.4155/tde.13.38.
27. Pourgholi F, Hajivalili M, Farhad JN, Kafil HS, Yousefi M. Nanoparticles: novel vehicles in treatment of glioblastoma. Biomed Pharmacother. 2016;77:98–107. https://doi.org/10.1016/j.biopha.2015.12.014.
28. Mujokoro B, Adabi M, Sadroddiny E, Adabi M, Khosravani M. Nano-structures mediated co-delivery of therapeutic agents for glioblastoma treatment: a review. Mater Sci Eng C. 2016;69:1092–102. https://doi.org/10.1016/j.msec.2016.07.080.
29. Ferreira NN, Caetano BL, Boni FI, Sousa F, Magnani M, Sarmento B, et al. Alginate-based delivery systems for bevacizumab local therapy: in vitro structural features and release properties. J Pharm Sci. 2018;108:1559–68. https://doi.org/10.1016/j.xphs.2018.11.038.
30. Wen Z, Yan Z, Hu K, Pang Z, Cheng X, Guo L, et al. Odorranalectin-conjugated nanoparticles: preparation, brain delivery and pharmacodynamic study on Parkinson's disease following intranasal administration. J Control Release. 2011;151:131–8. https://doi.org/10.1016/j.jconrel.2011.02.022.
31. Kumar M, Pandey RS, Patra KC, Jain SK, Soni ML, Dangi JS, et al. Evaluation of neuropeptide loaded trimethyl chitosan nanoparticles for nose to brain delivery. Int J Biol Macromol. 2013;61:189–95. https://doi.org/10.1016/j.ijbiomac.2013.06.041.
32. Crowe TP, Greenlee MHW, Kanthasamy AG, Hsu WH. Mechanism of intranasal drug delivery directly to the brain. Life Sci. 2018;195:44–52. https://doi.org/10.1016/j.lfs.2017.12.025.
33. Genchi GG, Marino A, Tapeinos C, Ciofani G. Smart materials meet multifunctional biomedical devices: current and prospective implications for nanomedicine. Front Bioeng Biotech. 2017;5:80. https://doi.org/10.3389/fbioe.2017.00080.
34. Yu S, Xu X, Feng J, Liu M, Hu K. Chitosan and chitosan coating nanoparticles for the treatment of brain disease. Int J Pharm. 2019;560:282–93. https://doi.org/10.1016/j.ijpharm.2019.02.012.
35. Bonaccorso A, Musumeci T, Serapide MF, Pellitteri R, Uchegbu IF, Puglisi G. Nose to brain delivery in rats: effect of surface charge of rhodamine B labeled nanocarriers on brain subregion localization. Colloid Surface B. 2017;154:297–306. https://doi.org/10.1016/j.colsurfb.2017.03.035.
36. Sanna V, Roggio AM, Siliani S, Piccinini M, Marceddu S, Mariani A, et al. Development of novel cationic chitosan-and anionic alginate-coated poly(D,L-lactide-co-glycolide) nanoparticles for controlled release and light protection of resveratrol. Int J Nanomedicine. 2012;7:5501–16. https://doi.org/10.2147/IJN.S36684.
37. Miranda-Goncalves V, Honavar M, Pinheiro C, Martinho O, Pires MM, Pinheiro C, et al. Monocarboxylate transporters (MCTs) in gliomas: expression and exploitation as therapeutic targets. Neuro-oncology. 2013;15:172–88. https://doi.org/10.1093/neuonc/nos298.
38. Miranda-Goncalves V, Cardoso-Carneiro D, Valbom I, Cury FP, Silva VA, Granja S, et al. Metabolic alterations underlying bevacizumab therapy in glioblastoma cells. Oncotarget. 2017;8:103657–70. https://doi.org/10.18632/oncotarget.21761.
39. Martinho O, Silva-Oliveira R, Cury FP, Barbosa AM, Granja S, Evangelista AF, et al. HER family receptors are important theranostic biomarkers for cervical cancer: blocking glucose metabolism enhances the therapeutic effect of HER inhibitors. Theranostics. 2017;7:717–32. https://doi.org/10.7150/thno.17154.

40. Silva-Oliveira RJ, Melendez M, Martinho O, Zanon MF, de Souza VL, Carvalho AL, et al. AKT can modulate the in vitro response of HNSCC cells to irreversible EGFR inhibitors. Oncotarget. 2017;8:53288–301. https://doi.org/10.18632/oncotarget.18395.
41. Park AK, Francis JM, Park WY, Park JO, Cho J. Constitutive asymmetric dimerization drives oncogenic activation of epidermal growth factor receptor carboxyl-terminal deletion mutants. Oncotarget. 2015;6:8839–50. https://doi.org/10.18632/oncotarget.3559.
42. Combs SE, Schulz-Ertner D, Roth W, Herold-Mende C, Debus J, Weber K-J. In vitro responsiveness of glioma cell lines to multimodality treatment with radiotherapy, temozolomide, and epidermal growth factor receptor inhibition with cetuximab. Int J Radiat Oncol Biol Phys. 2007;68:873–82. https://doi.org/10.1016/j.ijrobp.2007.03.002.
43. Samaridou E, Alonso MJ. Nose-to-brain peptide delivery—the potential of nanotechnology. Bioorg Med Chem. 2018;26:2888–905. https://doi.org/10.1016/j.bmc.2017.11.001.
44. Gao X, Wu B, Zhang Q, Chen J, Zhu J, Zhang W, et al. Brain delivery of vasoactive intestinal peptide enhanced with the nanoparticles conjugated with wheat germ agglutinin following intranasal administration. J Control Release. 2007;121:156–67. https://doi.org/10.1016/j.jconrel.2007.05.026.
45. Migliore MM, Vyas TK, Campbell RB, Amiji MM, Waszczak BL. Brain delivery of proteins by the intranasal route of administration: a comparison of cationic liposomes versus aqueous solution formulations. J Pharm Sci. 2010;99:1745–61. https://doi.org/10.1002/jps.21939.
46. Xia H, Gao X, Gu G, Liu Z, Zeng N, Hu Q, et al. Low molecular weight protamine-functionalized nanoparticles for drug delivery to the brain after intranasal administration. Biomaterials. 2011;32(36):9888–98. https://doi.org/10.1016/j.biomaterials.2011.09.004.
47. Mittal D, Ali A, Md S, Baboota S, Sahni JK, Ali J. Insights into direct nose to brain delivery: current status and future perspective. Drug Deliv. 2014;21:75–86. https://doi.org/10.3109/10717544.2013.838713.
48. Martínez Rivas CJ, Tarhini M, Badri W, Miladi K, Greige-Gerges H, Nazari QA, et al. Nanoprecipitation process: from encapsulation to drug delivery. Int J Pharm. 2017;532(1):66–81. https://doi.org/10.1016/j.ijpharm.2017.08.064.
49. Rao JP, Geckeler KE. Polymer nanoparticles: preparation techniques and size-control parameters. Prog Polym Sci. 2011;36:887–913. https://doi.org/10.1016/j.progpolymsci.2011.01.001.
50. Gao H. Progress and perspectives on targeting nanoparticles for brain drug delivery. Acta Pharm Sin B. 2016;6:268–86. https://doi.org/10.1016/j.apsb.2016.05.013.
51. Badran MM, Mady MM, Ghannam MM, Shakeel F. Preparation and characterization of polymeric nanoparticles surface modified with chitosan for target treatment of colorectal cancer. Int J Biol Macromol. 2017;95:643–9. https://doi.org/10.1016/j.ijbiomac.2016.11.098.
52. Bilati U, Allémann E, Doelker E. Development of a nanoprecipitation method intended for the entrapment of hydrophilic drugs into nanoparticles. Eur J Pharm Sci. 2005;24:67–75. https://doi.org/10.1016/j.ejps.2004.09.011.
53. Kaszuba M, Corbett J, Watson FM, Jones A. High-concentration zeta potential measurements using light-scattering techniques. Philos Trans Royal Soc A. 2010;368:4439–51. https://doi.org/10.1098/rsta.2010.0175.
54. Bento D, Staats HF, Goncalves T, Borges O. Development of a novel adjuvanted nasal vaccine: C48/80 associated with chitosan nanoparticles as a path to enhance mucosal immunity. Eur J Pharm Biopharm. 2015;93:149–64. https://doi.org/10.1016/j.ejpb.2015.03.024.
55. Schatz C, Domard A, Viton C, Pichot C, Delair T. Versatile and efficient formation of colloids of biopolymer-based polyelectrolyte complexes. Biomacromolecules. 2004;5:1882–92. https://doi.org/10.1021/bm049786+.
56. Pinto Reis C, Neufeld RJ, Ribeiro AJ, Veiga F. Nanoencapsulation I. Methods for preparation of drug-loaded polymeric nanoparticles. Nanomedicine. 2006;2:8–21. https://doi.org/10.1016/j.nano.2005.12.003.
57. Barichello JM, Morishita M, Takayama K, Nagai T. Encapsulation of hydrophilic and lipophilic drugs in PLGA nanoparticles by the nanoprecipitation method. Drug Dev Ind Pharm. 1999;25:471–6. https://doi.org/10.1081/DDC-100102197.
58. Bhattacharjee S. DLS and zeta potential—what they are and what they are not? J Control Release. 2016;235:337–51. https://doi.org/10.1016/j.jconrel.2016.06.017.
59. Vilaça N, Amorim R, Martinho O, Reis RM, Baltazar F, Fonseca AM, et al. Encapsulation of α-cyano-4-hydroxycinnamic acid into a NaY zeolite. J Mater Sci. 2011;46:7511–6. https://doi.org/10.1007/s10853-011-5722-2.
60. Wang Y, Li P, Kong L. Chitosan-modified PLGA nanoparticles with versatile surface for improved drug delivery. AAPS PharmSciTech. 2013;14:585–92. https://doi.org/10.1208/s12249-013-9943-3.
61. Mourya V, Inamdar NN. Trimethyl chitosan and its applications in drug delivery. J Mater Sci Mater Med. 2009;20:1057–79. https://doi.org/10.1007/s10856-008-3659-z.
62. de Britto D, de Moura MR, Aouada FA, Mattoso LH, Assis OB. N, N, N-trimethyl chitosan nanoparticles as a vitamin carrier system. Food Hydrocoll. 2012;27:487–93. https://doi.org/10.1016/j.foodhyd.2011.09.002.
63. Kang B-S, Choi J-S, Lee S-E, Lee J-K, Kim T-H, Jang WS, et al. Enhancing the in vitro anticancer activity of albendazole incorporated into chitosan-coated PLGA nanoparticles. Carbohydr Polym. 2017;159:39–47. https://doi.org/10.1016/j.carbpol.2016.12.009.
64. Schubert S, Delaney JT Jr, Schubert US. Nanoprecipitation and nanoformulation of polymers: from history to powerful possibilities beyond poly (lactic acid). Soft Matter. 2011;7:1581–8. https://doi.org/10.1039/c0sm00862a.
65. Vu-Quang H, Vinding MS, Xia D, Nielsen T, Ullisch MG, Dong M, et al. Chitosan-coated poly (lactic-co-glycolic acid) perfluorooctyl bromide nanoparticles for cell labeling in 19F magnetic resonance imaging. Carbohydr Polym. 2016;136:936–44. https://doi.org/10.1016/j.carbpol.2015.09.076.
66. Manjappa AS, Chaudhari KR, Venkataraju MP, Dantuluri P, Nanda B, Sidda C, et al. Antibody derivatization and conjugation strategies: application in preparation of stealth immunoliposome to target chemotherapeutics to tumor. J Control Release. 2011;150:2–22. https://doi.org/10.1016/j.jconrel.2010.11.002.
67. Nel AE, Madler L, Velegol D, Xia T, Hoek EMV, Somasundaran P, et al. Understanding biophysicochemical interactions at the nano-bio interface. Nat Mater. 2009;8:543–57. https://doi.org/10.1038/nmat2442.
68. Ferreira NN, Ferreira LMB, Miranda-Gonçalves V, Reis RM, Seraphim TV, Borges JC, et al. Alginate hydrogel improves anti-angiogenic bevacizumab activity in cancer therapy. Eur J Pharm Biopharm. 2017;119:271–82. https://doi.org/10.1016/j.ejpb.2017.06.028.
69. Naahidi S, Jafari M, Edalat F, Raymond K, Khademhosseini A, Chen P. Biocompatibility of engineered nanoparticles for drug delivery. J Control Release. 2013;166(2):182–94. https://doi.org/10.1016/j.jconrel.2012.12.013.
70. Amorim R, Vilaça N, Martinho O, Reis RM, Sardo M, Rocha J, et al. Zeolite structures loading with an anticancer compound as drug delivery systems. J Phys Chem C. 2012;116:25642–50. https://doi.org/10.1021/jp3093868.
71. Halestrap AP, Denton RM. Specific inhibition of pyruvate transport in rat liver mitochondria and human erythrocytes by alpha-cyano-4-hydroxycinnamate. Biochem J. 1974;138:313–6. https://doi.org/10.1042/bj1380313.